Research Article

Chemical Review and Letters
journal homepage: www.chemrevlett.com
ISSN (online): 2645-4947 (print) 2676-7279

Thioindole adsorption as a biologically active anticancer over C_{20} fullerene in different reaction media using density functional theory

Marziyeh Mohammadi [1,*], Fahimeh Alirezapour [2]

[1]*Department of Chemistry, Faculty of Science, Vali-e-Asr University of Rafsanjan, Rafsanjan, Iran*
[2]*Department of Chemistry, Payame Noor University (PNU), P.O. Box 19395-4697, Tehran, Iran*

ARTICLE INFO

Article history:
Received 19 January 2024
Received 21 February 2024
Accepted 21 February 2024
Available online 21 February 2024

Keywords:
Solvent
Complex
TS
Stability
Hollow cage

ABSTRACT

The adsorption of the pyrrole-thioindole **(1)** and C_{20} cage **(2)** are studied at B3LYP/6-311+G*, B3LYP/6-311++G** and B3LYP/AUG-cc-pVTZ. Stability of solute and complex **(3)** depends on the dielectric constant of the used solvent (ε), the possibility of the hydrogen bonding (H…B) and dipolar–dipolar interaction (D.-D.I.) between them. In going from the gas phase to less polar solvent, then in turn to more polar solvent, a good consistency appears between ε and the absolute value of adsorption energy difference among solvent phase and gas phase *i.e.* $|\Delta E_{\text{ads. of s-g}}|$ obtained for product **(3)**. Moreover, the highest $|\Delta E_{\text{ads. of s-g}}|$ is measured for **(3)** in water, whereas the lowest value is associated in cyclohexane. Because of capability of (H…B), **(3)** is stabilized in the most polar solvent (water) more than gas phase and other solvents. The kinetic stability and energy difference between the frontier orbitals (E_g or $\Delta E_{\text{L-H}}$) is observed in the opposite direction with ε. A red shift is monitored when adsorption is taken in polar solvents as $\Delta E_{\text{L-H}}$ is reduced.

1. Introduction

In the last decades, the indole and thioindole's derivatives have been investigated, as potent and selective inhibitor against different receptor tyrosine kinase [1-7].

Solvent effects on physical or chemical processes are usually studied by means of empirical solvent parameters. The SCRF theory has been applied to many problems using both semi-empirical and/or *ab initio* methods [8]. Not only owing to water exhibits unique selectivity as well as reactivity, which is diverse from those in conventional organic solvents; but also due to it is as the most inexpensive, plenteous, along with environmentally friendly solvent. Consequently, the improvement of novel selectivity along with reactivity that cannot be realized in predictable organic solvents is one of the challenging purposes of aqueous chemistry.
Nanomaterials such pure and/or the doped—nanotubes, cyclacenes, polyacenes, nanographene, nanosheets, nanocones, nanocages (fullerenes) and so on have been widely studied for adsorbing and sensing drugs and biomolecules [9-12]. Most adsorption reactions to nanostructures are accomplished under thermal conditions, but photochemical reactions have been reported; also various microwave irradiations can be used as source of energy. Indeed, functionalization, encapsulation, substitution, and adsorption of these nanostructures by cationes, aniones, heteroatoms and biologically active heterocyclic compounds has been object of experimental and computational investigations expected at understanding the stability, structural, chemical reactivity, electronic and magnetic possessions of the resulted structures [13-14].

Although functionalization of larger fullerenes using organic methodologies has been well established; because of their low solubility in organic solvents, functionalization of smaller fullerenes and their processibility have been relatively poor developed [13-14]. Reaction of the indole derivatives with C_{60} cage, has been reported under microwave irradiation or

∗ Corresponding author.; e-mail: m.mohammadi@vru.ac.ir
https://doi.org/ 10.22034/crl.2024.436695.1284

thermal conditions [6], also solubility of C_{60} has been studied experimentally in a wide variety of solvents; while owing to extreme curvature and reactivity of the dodecahedral fullerene (**C_{20}**; **2**), this obscure molecule has been subject of many theoretical investigations [9,15]. Despite labile nature of the mentioned structure (**C_{20}**; **2**), as the smallest possible fullerene, its successful production is accomplished *via* stable dodecahedrane ($C_{20}H_{20}$) in gas phase on the microsecond-scale lifetime. Interestingly, due to Jahn–Teller distortion, extreme π-curvature, high strain and unstability of **(2)**, search for its stable analogues, namely heterofullerene and organofullerene, becomes appealing [9,15].

Here, we have employed the DFT-SCRF to research the effects of different solvents on the structure, stability and stereoselective adsorption of diene **(1)** to dienophile **(2)**, for complex formation of (*E*)-3-1H-pyrrole-2-ylindoline-2-thione[20]fullerene **(3)** (Figure 1) [9,15].

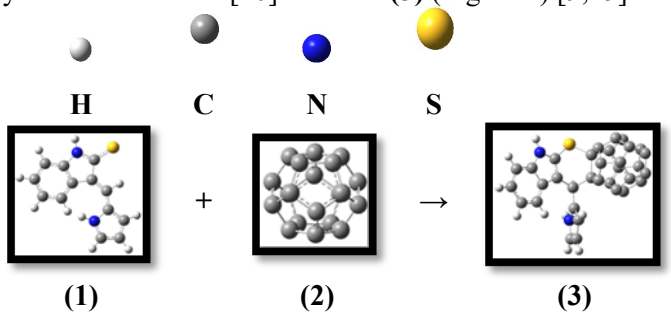

Fig. 1. Structures of the scrutinized adsorption.

2. Computational Methods

Full optimization of **(1)**, **(2)**, and **(3)** minima as well as transition states of **TS-I** and **TS-II** are completed without any symmetry constraints by means of three-parameter hybrid functional proposed by Becke (B3) and correlation functional suggested by Lee–Yang–Parr (LYP), Pople's well-known basis set (6-311+G*) and an extra plus due to the importance of diffuse functions, employing the GAMESS program package [16-18]. The **TS-I** and **TS-II** calculations are performed using the reactants-products quadratic-synchronous transit (QST3) algorithm [19]. For **(1)**, **(2)**, and **(3)** minima only real frequency values (with a positive sign); also for **TS-I** and **TS-II** structures, only a single imaginary frequency value (with a negative sign) is accepted. To obtain more accurate energetic data, single point calculations are performed at B3LYP/6-311++G** and B3LYP/AUG-cc-pVTZ [20]. The AIM, NBO, MEP analysis is carried out at the same method and level (See Supplementary Information) [21].

Employing the notation of Xantheas [22], the adsorption energy ($E_{ads.}$) is obtained *via* the following equation:

$$E_{ads.} = E_{(3)} - (E_{(1)} + E_{(2)}) + E_{BSSE} \quad (1)$$

$$\left|\Delta E_{ads.\ of\ s\text{-}g}\right| = \left|E_{ads.\ in\ the\ liquid\ phase} - E_{ads.\ in\ the\ gas\ phase}\right| \quad (2)$$

Here, $E_{(3)}$ is expected as energy of the **(1)**/**(2)** complex; when **(1)** is adsorbed on **(2)**, $E_{(1)}$ is energy of the molecule **(1)**, and $E_{(2)}$ is energy of the cage **(2)**. The negative adsorption energy shows that this absorption is an exothermic process. The HOMO/LUMO energy gap (E_g or $\Delta E_{L\text{-}H}$) is found according to the following equation:

$$E_g = E_{LUMO} - E_{HOMO} \quad (3)$$

In order to obtain computed UV spectra, we are used the TD-DFT method, the functional, basis set, and number of the allowed transitions by # TD=(50-50, nstates=10, root=1) B3LYP/AUG-cc-pVTZ scrf=(cpcm, solvent=water) kywords.

3. Results and Discussion

3.1. Energy, geometry, and AIM analysis

To get suitable and stable ground state of **(1)**, **(2)**, **(3)** minima, **TS-I** and **TS-II**, force constant calculations are done, where **(1)**, **(2)**, **(3)** minima exhibit the positive force constants, while **TS-I** and **TS-II** exhibit one negative force constant. In order to check the reliability of the **TS-I** and **TS-II** with the reactants **(1, 2)** and the desired product **(3)**, IRC calculations must be performed, accordingly (Schemes S١ and S٢).

One of important macroscopic properties of solvent molecules is ε as good indicator for indicating the ability to accommodate separation of the positive and negative charge [1-7]. Here, solvents with large ε (*e.g.* H_2O, DMSO, acetonitrile, and MeOH) are compared and are contrasted to solvents with small ε (*e.g.* chloroform, and cyclohexane) (Figures 2 and 3).

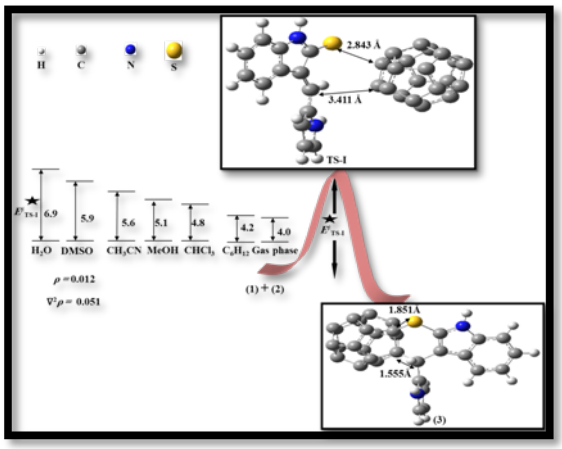

Fig. 2. The optimized structures, $E^{\neq}_{TS\text{-}I}$ (in kcal/mol) and AIM (atoms in molecules) parameters including the charge density (ρ) and the Laplacian of the charge density ($\nabla^2\rho$) for adsorption of **(1)** with **(2)** *via* **TS-I**, in different reaction media.

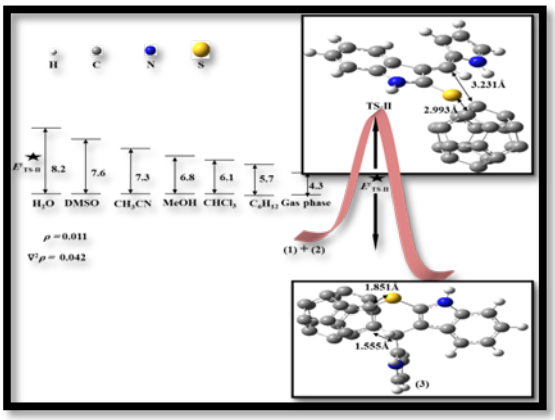

Fig. 3. The optimized structures, $E^{\neq}_{TS\text{-}II}$ (in kcal/mol) and AIM parameters for adsorption of **(1)** with **(2)** *via* **TS-II**, in different reaction media.

Obviously, the stabilizing effect of more polar solvents on **TS-I**, **TS-II** and complex **(3)** is more than less polar solvents of cyclohexane and chloroform. Hence, the $E^{\neq}_{TS\text{-}I}$ is decreased from 6.9 (in H_2O) to 5.9 (in DMSO), 5.6 (in acetonitrile), 5.1 (in MeOH), 4.8 (in chloroform), 4.2 (in cyclohexane) and 4.0 kcal/mol (in gas phase), respectively, Also, the $E^{\neq}_{TS\text{-}II}$ trend is found somewhat higher than $E^{\neq}_{TS\text{-}I}$ trend; and the $E^{\neq}_{TS\text{-}II}$ is diminished from 8.2 (in H_2O) to 7.6 (in DMSO), 7.3 (in acetonitrile), 6.8 (in MeOH), 6.1 (in chloroform), 5.7 (in cyclohexane) and 4.3 kcal/mol (in gas phase), respectively. Apparently, the highest activation energy is related to adsorption *via* endo orientation, the possibility of (H…B) and (D.-D.I.) in H_2O, whereas the lowest activation energy is associated with exo orientation, the impossibility of (H…B) and (D.-D.I.) in gas phase. Endo orientation along with formation of the endo conformer is anticipated to be less favorable because of π-π stacking between the substituted pyrrole ring and $\mathbf{C_{20}}$ ($\pi_{\text{pyrrole}} \leftrightarrow \pi_{C20}$) [23].

Full optimized geometry of **TS-I** and **TS-II** dictates stability of the complex **(3)**; so that the torsion angle of the substituted pyrrole ring and C=S in **TS-I**, **TS-II**, and complex **(3)** is 0.5°, 1.0° and 90.5°, correspondingly. This ring vertically produces an enormous steric hindrance *vs.* the endo-oriented attack to the cage **(2)**. Henceforth, the endo conformer involves higher energy than the exo conformer. Also, there is higher possibility for non-bonding electrons of nitrogen in thioindole skeleton of **(1)** to conjugation with the neighboring C=S group that may be recognized to the planarity between the thioindoline structure and the substituted pyrrole ring of **TS-I** and **TS-II** [1-7]. The distance among the thioindoline skeleton and nanocage of **TS-I** (3.411, and 2.843 Å) is dissimilar to that of **TS-II** (2.231, and 0.663 Å) which depends on interaction between **(1)** and solvent. The bond length difference is somewhat large, and TS structures are obviously consistent with the concerted synergistic reaction mechanism, which is in accordance with Diels–Alder mechanism. Probably, dienophile **(2)** is set vertically between two double-bonds of diene **(1)** and hence adsorption is take placed from two different faces of **(2)**, thus the pyrrole ring and the nanocage **(2)** are cis to each other.

Geometry of **(3)** complex appears to some extent different in gas phase and other reaction media. The distance between **a** and **c** rings (Scheme 1) is 3.006 Å in the gas phase; while in the used solvents is about 2.456 to 2.790 Å, which indicates D.-D.I. among solute and $CHCl_3$, MeOH, acetonitrile, DMSO, and H_2O solvents.

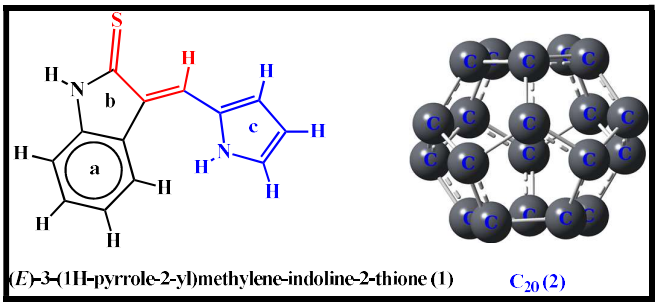

Scheme 1. The structures of **(1)** and **(2)**.

The bond length (B.L.) and bond angle (B.A.) between **a** and **c** rings of **(3)** complex in the gas phase and cyclohexane are compared to one of the (H…B) donor and (H…B)—acceptor solvents such as H_2O, MeOH, and $CHCl_3$. The largest discrepancy of B.L. and B.A. is less than 0.216, 0.431, and 0.550 Å; 4.1, 3.9, and 4.0°, respectively (Tables S1 and S2).

These minor discrepancies may be due to intermolecular interaction between the N—H moiety of **(3)** complex and the H—O of solvent, but theoretical calculations belong to the single molecules. There are inter-molecular H…B (inter-H…B) in the aqueous phase or alcoholic solvent, such as N-H···O. For solvation in MeOH; because the inter-(H…B) bond length is 2.790 Å, the B.L. value of proton donor N—H is 1.052 Å, and the interatomic distance of H···O is 1.679 Å. For solvation in water, the B.L. value of the N—H···O is 2.615 Å, the B.L. value of N—H is 1.029 Å, and the interatomic distance of H···O is 1.456 Å. The obtained B.L. value in the aqueous phase is in better agreement with the experimental ones, further demonstrating the significance of solvent effect. The B.A. value of N—H···O in MeOH, and water is 153.7° and 164.0°, respectively. Ideally, the B.L. value of (H…B) is close to 180°, but the steric hindrance or the competition of other forces would influence the B.A. value. As a whole, the (H…B) bond angles are larger than 90° and

less than 180°. The mentioned evidences in above illustrate that the hydrogen bond formation in N—H···O moiety of a system is an inter-H…B.

In going from gas phase to the different solvents, variations of torsion angle (T.A.) occur especially for T.A. (10,26,38,39), T.A. (10,26,38,40), T.A. (23,26,38,39), T.A. (23,26,38,40), T.A. (10,26,38,45), and T.A. (23,26,38,45) which these torsion angles are confirmed between the substituted pyrrole ring, and the cyclohexene ring of complex **(3)** (Table 1).

The AIM analysis containing ρ of 0.012, 0.011 *a.u.* and $\nabla^2\rho$ of 0.051, 0.042 *a.u.*, is estimated for **TS-I** and **TS-II**, respectively, which reveals (D.-D.I.) between the substituted pyrrole ring of diene **(1)** and the π system of dienophile **(2)** also the resulted π-π stacking. Clearly, positive value of $\nabla^2\rho$ indicates electrostatic interaction existing in **TS-I** is more than **TS-II**.

The π-π stacking of **TS-II** shows distance between the thioindoline skeleton **(1)** and fullerene **(2)** in the range of 2.99 – 3.96 Å, which is consistent with the observed π-π aromatic interaction in experimental investigation [23]. They appear to these phenomena have lower stabilizing effects on the studied TS for adsorption *via* the endo-oriented attack compared to the exo-oriented attack.

3.2. Stability analysis

The trend of $|\Delta E_{\text{ads. of s-g}}|$ in kcal/mol for complex **(3)** is estimated as $|\Delta E_{\text{ads. of cyclohexane - gas phase}}|$ [7.17] < $|\Delta E_{\text{ads. of chloroform - gas phase}}|$ [11.59] < $|\Delta E_{\text{ads. of methanol - gas phase}}|$ [12.65] < $|\Delta E_{\text{ads. of acetonitrile - gas phase}}|$ [13.25] < $|\Delta E_{\text{ads. of DMSO - gas phase}}|$ [15.39] < $|\Delta E_{\text{ads. of water - gas phase}}|$ [17.44]; also the trend of ε is followed as $\varepsilon_{\text{gas phase}}$ [1] < $\varepsilon_{\text{cyclohexane}}$ [2.0] < $\varepsilon_{\text{chloroform}}$ [4.8] < $\varepsilon_{\text{methanol}}$ [32.6] < $\varepsilon_{\text{acetonitrile}}$ [36.6] < $\varepsilon_{\text{DMSO}}$ [46.7] < $\varepsilon_{\text{water}}$ [78.4] (Figure 4).

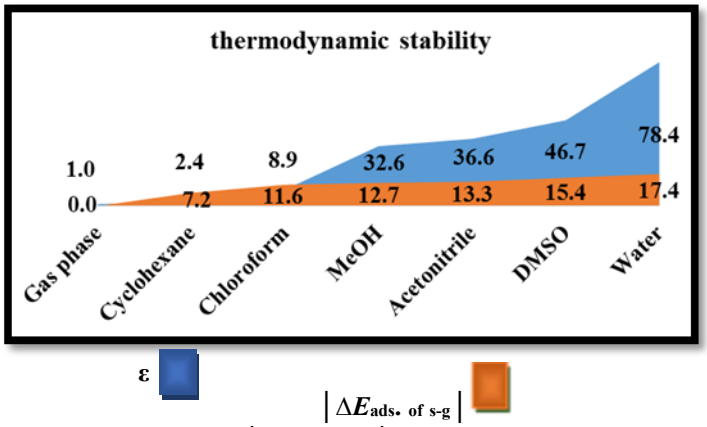

Fig. 4. Comparison of $|\Delta E_{\text{ads. of s-g}}|$ in kcal/mol and ε, for the scrutinized adduct **(3)** in different reaction media.

Thus, the trend of $|\Delta E_{\text{ads. of s-g}}|$ is convenient and is parallel to the trend of ε. In going from the gas phase to less polar solvent, and in turn to more polar solvent, a suitable consistency seems between the ε of solvent and thermodynamic stability of complex **(3)** (Figure 5).

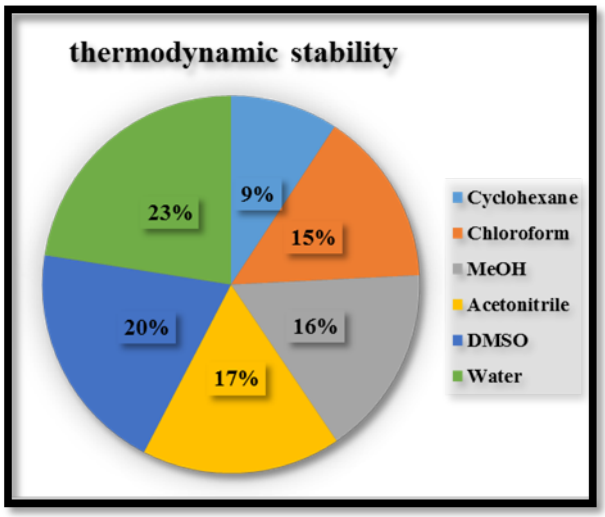

Fig. 5. The solvent effect on $|\Delta E_{\text{ads. of s-g}}|$ of the scrutinized adduct **(3)**.

Moreover, the highest value of the released $\Delta E_{\text{ads. of s-g}}$; -17.44 kcal/mol and the most thermodynamic stability is observed for the optimized complex **(3)** in water (23%), whereas the lowest value of -7.17 kcal/mol is estimated in cyclohexane (9%). The dipole moment (μ) of **(3)** in solution changes regularly with increasing of ε: $\mu_{\text{in gas phase}}$ [5.05 D] < $\mu_{\text{in cyclohexane}}$ [5.80 D] < $\mu_{\text{in chloroform}}$ [6.15 D] < $\mu_{\text{in methanol}}$ [6.71 D] < $\mu_{\text{in acetonitrile}}$ [7.22 D] < $\mu_{\text{in DMSO}}$ [7.90 D] < $\mu_{\text{in water}}$ [8.96 D]. Hence, more polar solvent decreases the energy of **(3)** through salvation by D.-D.I. and H…B (Figure 6).

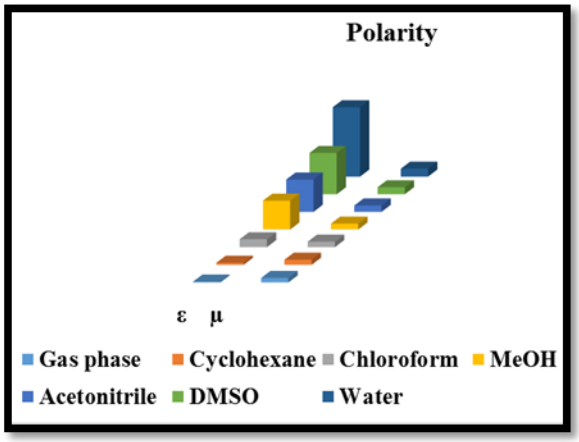

Fig. 6. The solvent effects on polarity of the scrutinized adduct **(3)**.

Since thioindole **(1)** as a 1,3-diene is inherently either an electrophile or a nucleophile, simultaneous inter-molecular HOMO-LUMO interaction of it with hollow cage **(2)** as dienophile leads to the suggested adsorption through either the filled π_2-orbital of **(1)** with the vacant π^*_2-orbital of **(2)**, or the filled π_1-orbital of **(2)** with the vacant π^*_3-orbital of **(1)** (Figure 7).

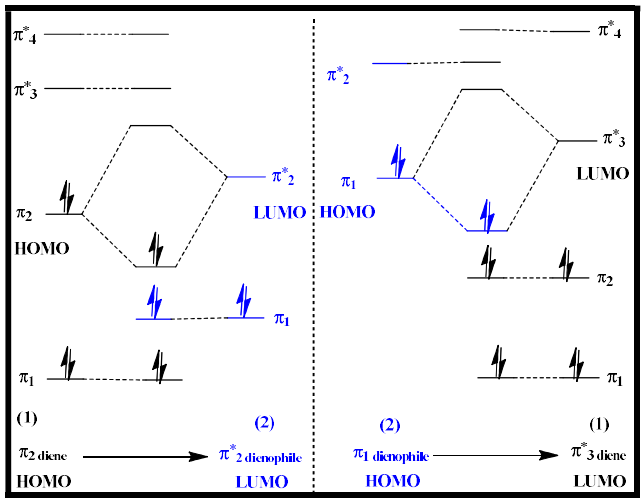

Fig. 7. Inter-molecular HOMO-LUMO interactions of **(1)** as diene, with **(2)** as dienophile.

Furthermore, the trend of E_g or $\Delta E_{L\text{-}H}$ in eV for complex **(3)** is emerged in the opposite direction with the trend of ε and polarity of the solvent: 2.08 (in H_2O) < 2.12 (in DMSO) < 2.16 (in acetonitrile) < 2.23 (in MeOH) < 2.29 (in $CHCl_3$) < 2.32 (in cyclohexane) < 2.53 (in gas phase) (Table 1).

Table 1. The highest occupied and the lowest unoccupied molecular orbital energies (E_{HOMO} and E_{LUMO}) / hartree, and the energy differences between them ($\Delta E_{L\text{-}H}$) / eV, for the complex **(3)**, in different reaction media, at B3LYP/AUG-cc-pVTZ.

Solvents	E_{HOMO} (*a.u.*)	E_{LUMO} (*a.u.*)	$\Delta E_{L\text{-}H}$ (eV)
gas phase	-0.1973	-0.1043	2.53
cyclohexane	-0.2090	-0.1238	2.32
$CHCl_3$	-0.2091	-0.1248	2.29
MeOH	-0.2071	-0.1250	2.23
acetonitrile	-0.2043	-0.1250	2.16
DMSO	-0.2031	-0.1250	2.12
H_2O	-0.2013	-0.1250	2.08

The complex **(3)** is shown the lowest and the highest $\Delta E_{L\text{-}H}$ of 2.08 and 2.53 eV in H_2O and gas phase, respectively [. This complex such as the Kekule´ other compounds enjoys from resonance and full conjugation; so that it shows good band gap in gas phase and in cyclohexane; while it exhibits relatively narrow band gap in $CHCl_3$, MeOH, acetonitrile, DMSO, and H_2O, which low $\Delta E_{L\text{-}H}$ leads to high chemical reactivity in polar solvents (Figure 8).

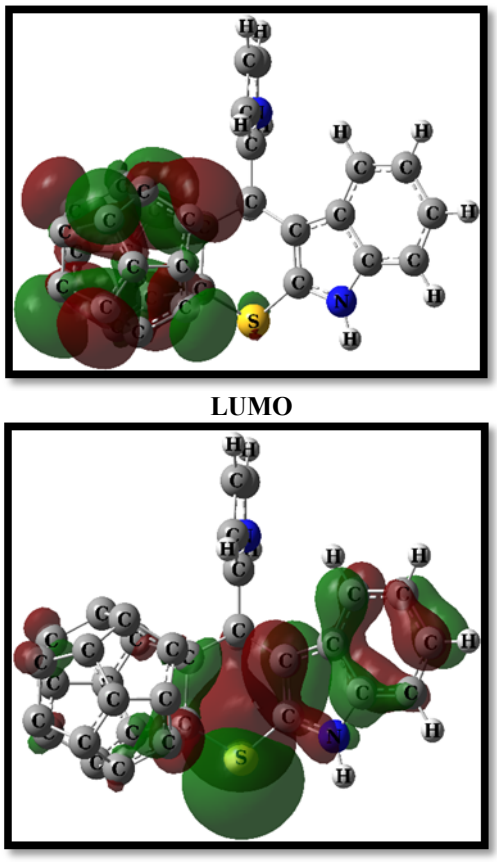

Fig. 8. The HOMO and LUMO shapes of the complex **(3)**.

The HOMO profile shown in Figure 8 confirms that the HOMO of complex **(3)** is shifted on the cyclohexene and indoline-2-thione moiety with changing the HOMO energy [24-26]. Also, the LUMO profile of complex **(3)** is shifted on it's hollow cage **(2)** with changing the LUMO energy. In going from the gas phase to every less polar solvent, then in turn to every more polar solvent, individually, the HOMO energy changes to a greater extent than the LUMO energy. We have found that the solvent effect and stabilizing effect from gas phase to water causes to decreasing the HOMO energy of 0.004 *a.u.;* therefore, there is the opposite direction between order of E_g and order of ε (Figure 9) [24-27].
The reason for the difference in Figure 9 is more sensitive of the complex **(c)** to stabilizing effect of more polar solvent *via* (H…B) and (D.-D.I.) than less polar solvents or gas phase. According to the above discussion, another reason for the lower E_g ($\Delta E_{L\text{-}H}$) in the aqueous phase than the gas phase may be the presence of inter-H…B.

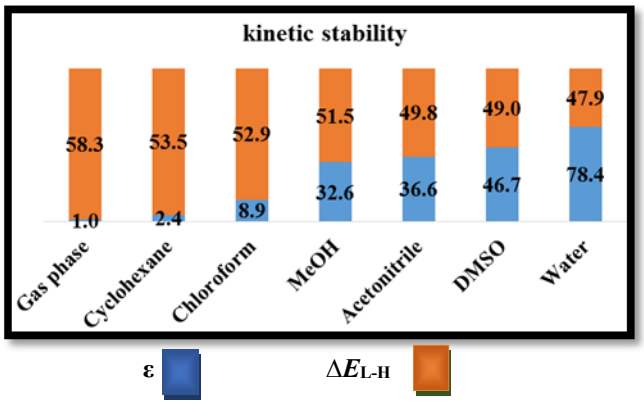

Fig. 9. Comparison of ε and the energy gap between HOMO and LUMO ($\Delta E_{L\text{-}H}$) in kcal/mol of the scrutinized adduct **(3)** in different reaction media.

3.3. UV-vis, NBO, and MEP analysis

Examining the UV-visible spectrum of a molecule in the H…B donor and H…B—acceptor solvent will be useful in detecting inter-H…B. Herein, the absorption spectra of the complex **(c)** are investigated in the corresponding reaction media (with relative polarity in parenthesis) including gas phase (0.000), C_6H_{12} (0.006), $CHCl_3$ (0.259), MeOH (0.762), and H_2O (1.000) to correlate the effect of solvent polarity on absorption in the UV-visible region. The wavelength at maximum absorption (λ_{max}) of the scrutinized product is measured in some solvents with diverse polarity. The λ_{max} of the complex **(c)** is displayed a tight range of 489.40-931.43 nm in gas phase, 502.63-993.08 nm in cyclohexane, and 504.08-994.52 nm in chloroform (Figure S1). It is changed from 504.41 to 1000.09 nm in methanol and from 504.80 to 1009.72 nm in water. Henceforth, a red shift is monitored when adsorption is taken in polar solvents as $\Delta E_{L\text{-}H}$ is reduced. The relationship between the change of λ_{max}, and polarity of the solvents can be summarized as:

(a) The λ_{max} value is higher in H_2O than the conforming values in MeOH, $CHCl_3$, C_6H_{12}, and gas phase. (b) The highest λ_{max} value is observed 1009.72 nm in H_2O. Thus, H_2O solvent creates more bathochromic shift than methanol, chloroform, cyclohexane and gas phase. (c) The pyrrole group's introduction at the complex **(c)** affects shifting the λ_{max} to higher value (bathochromic shift), in all solvents. (d) The fullerenic group's introduction at the complex **(c)** affects shifting the λ_{max} to lower values (hypsochromic shift), in all solvents. (e) We have found some differences in the absorption spectra of the complex **(c)** in the different reaction media. The $n\rightarrow\pi^*$ transition involving the heteroatom's lone pair is destabilized by a polar solvent like water, and it becomes the second excited state in solution displaying an important blue shift. The presence of the heteroatom atom modulates the solvent effect and the excited states become practically degenerate for adsorption process.

In continuous, NBO results are presented in more detail, including all of the charge transfer parameters, donor, acceptor fragments and their relevant energies. The NBO charge points out different orientation, different charge transfers and different bond strength between atoms of **TS-I**, **TS-II** and complex **(3)**. For example, the charge on S atom is -0.841, -0.904, +0.167 and the charge on fullerene C atom near to S atom is +0.557, +0.918, -0.229 of **TS-I**, **TS-II** and complex **(3)**, respectively (Figure S2). Obviously, higher charge transfer indicates higher donor-acceptor interaction in **TS-I**, **TS-II** and complex **(3)**.

To visualizing of the distributed charge, the MEP plots of these structures may be useful (Figure S3). Red colored MEP is related to the electron cloud and blue colored MEP is related to H and C atoms.

In going from the gas phase to aqueous phase, however, the interactions between donors and acceptors are changed, especially in water solvent. As a whole, the interaction energies ($E^{(2)}$) of the complex **(3)** in the gas phase are lower than those in the aqueous phase by about 0.5 – 1.5 kcal/mol (Table 2).

Table 2. Second order perturbation theory analysis for the most important acceptor-donor interaction ($E^{(2)}$ in kcal/mol) of the complex **(3)**, in gas phase and water, at B3LYP/AUG-cc-pVTZ.

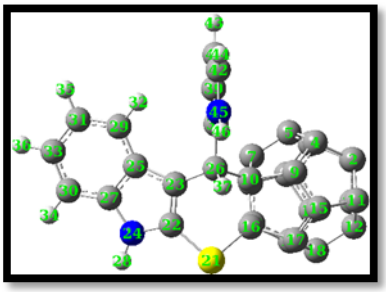

	interaction	$E^{(2)}$
gas phase	$\sigma_{C25-C27} \rightarrow \sigma^*_{N24-H28}$	2.01
	$\sigma_{C10-C26} \rightarrow \sigma^*_{C38-N45}$	1.72
	$\sigma_{C16-S21} \rightarrow \sigma^*_{C22-N24}$	1.98
	$\pi_{C17-C18} \rightarrow \sigma^*_{C16-S21}$	3.05
	$\pi_{C22-C23} \rightarrow \sigma^*_{C10-C26}$	1.04
	$\pi_{C22-C23} \rightarrow \sigma^*_{C16-S21}$	1.95
	$\sigma_{C23-C25} \rightarrow \sigma^*_{S21-C22}$	3.41
	$\sigma_{C26-C38} \rightarrow \sigma^*_{C10-C16}$	1.71
	$\sigma_{C26-C38} \rightarrow \sigma^*_{C10-C26}$	0.59
	$\sigma_{C38-C39} \rightarrow \sigma^*_{N45-H46}$	2.01
	$\pi_{C38-C39} \rightarrow \sigma^*_{C10-C16}$	0.44
	$\pi_{C38-C39} \rightarrow \sigma^*_{C10-C26}$	1.72
	$\sigma_{C38-N45} \rightarrow \sigma^*_{C10-C26}$	1.50

	$\sigma_{C42 - N45} \rightarrow \sigma^*_{C26 - C38}$	1.81
water	$\sigma_{C25 - C27} \rightarrow \sigma^*_{N24 - H28}$	2.69
	$\sigma_{C10 - C26} \rightarrow \sigma^*_{C38 - N45}$	2.50
	$\sigma_{C16 - S21} \rightarrow \sigma^*_{C22 - N24}$	2.71
	$\pi_{C17 - C18} \rightarrow \sigma^*_{C16 - S21}$	3.75
	$\pi_{C22 - C23} \rightarrow \sigma^*_{C10 - C26}$	1.88
	$\pi_{C22 - C23} \rightarrow \sigma^*_{C16 - S21}$	2.14
	$\sigma_{C23 - C25} \rightarrow \sigma^*_{S21 - C22}$	4.96
	$LP_{(O)} \rightarrow \sigma^*_{N24 - H28}$	21.22
	$\sigma_{C26 - C38} \rightarrow \sigma^*_{C10 - C16}$	2.11
	$\sigma_{C26 - C38} \rightarrow \sigma^*_{C10 - C26}$	1.10
	$\sigma_{C38 - C39} \rightarrow \sigma^*_{N45 - H46}$	2.69
	$\pi_{C38 - C39} \rightarrow \sigma^*_{C10 - C16}$	0.54
	$\pi_{C38 - C39} \rightarrow \sigma^*_{C10 - C26}$	2.15
	$\sigma_{C38 - N45} \rightarrow \sigma^*_{C10 - C26}$	2.51
	$\sigma_{C42 - N45} \rightarrow \sigma^*_{C26 - C38}$	2.82
	$LP_{(O)} \rightarrow \sigma^*_{N45 - H46}$	21.22

This indicates that the stability of the complex **(3)** in the aqueous phase is higher than in the gas phase. This may be attributed to the presence of inter-H…B in the aqueous phase. As shown in Table 3, inter molecular interactions mainly come from the delocalization of lone pair electrons of O—atom to σ* orbitals of N—H, which explains the nature of the formation of H…B in N—H···O. Comparison of the $E^{(2)}$ of $\sigma_{C25 - C27} \rightarrow \sigma^*_{N24 - H28}$, $\sigma_{C38 - C39} \rightarrow \sigma^*_{N45 - H46}$, $LP_{(O)} \rightarrow \sigma^*_{N24 - H28}$ and $LP_{(O)} \rightarrow \sigma^*_{N45 - H46}$ interactions shows that two formers are lower (about 10 times) than two latters by 2.01 kcal/mol in the gas phase, 2.69 kcal/mol in water *vs.* 21.22 kcal/mol in water, suggesting the most important interaction; inter-H…B of N—H···O in water solvent. A hydrogen-bonding energy of 7.6 kcal/mol has been determined experimentally for dimeric 2-pyrrolidone in CCl_4. This agrees well with the value of 21.22 kcal/mol (about three times) estimated for acceptor-donor interaction of the complex **(3)** in water with three inter-H…B sites. Also, in this solvent, the most intra molecular interactions are resulted from the bonding orbital of $\sigma_{C23 - C25}$ to the anti-bonding orbital of $\sigma^*_{S21 - C22}$; ($\sigma_{C23 - C25} \rightarrow \sigma^*_{S21 - C22}$), with the $E^{(2)}$ value of 4.96 kcal/mol, then from the bonding orbital of $\pi_{C17 - C18}$ to the anti-bonding orbital of $\sigma^*_{C16 - S21}$; ($\pi_{C17 - C18} \rightarrow \sigma^*_{C16 - S21}$) with $E^{(2)}$ of 3.75 kcal/mol.

Summarily, we found that "adsorption is more favorable in water than the gas phase" according to the NBO analysis. The question is: does the adsorption on C_{60} (crystal) occur in the gas phase? —The researcher easily prepared α,β-unsaturated indolin-2-thiones proved to be appropriate materials for the synthesis of macrocycle tetrahydrothiopyrano [2,3-b] indole—C_{60} derivatives *via* Diels–Alder reaction [6]. This reaction is applicable to buckyball, giving an irreversible product, and a C—S bond can be formed on it's surface. Organofullerenes are thermodynamically stable compounds because of the aromatic character of the resulting cycloadduct, thus avoiding the undesired cyclo-reversion process observed in other C_{60}-based [4+2] cycloaddition reactions [15]. In particular, various substituents can be introduced on the heterocycle by employing some kinds of reagents.

4. Conclusion

In this research, we have studied electronic effects on structural, thermodynamic and kinetic parameters of adsorption of anti-tumor **(1)** to hollow cage **(2)**, in gas phase, at DFT. To this end, the full optimization of complex **(3)** done in cyclohexane, $CHCl_3$, MeOH, acetonitrile, DMSO, and H_2O solvents, and the results compared and contrasted, too.

In going from gas phase to more polar solvent H_2O, the $E^{\neq}_{TS-I}$ increased from 4.0 to 6.9 kcal/mol and the $E^{\neq}_{TS-II}$ increased from 4.3 to 8.2 kcal/mol. The trend of $|\Delta E_{ads.\ of\ s\text{-}g}|$ and thermodynamic stability of complex **(3)** followed with dielectric constant of solvent (ε); from 7.2 kcal/mol in cyclohexane to 17.4 kcal/mol in H_2O. The polarity of complex **(3)** considerably changed from 5.1 Debye in gas phase to 9.0 Debye in water. The trend of ΔE_g or $\Delta E_{L\text{-}H}$ changed from 2.53 eV in gas phase to 2.08 eV in H_2O which arranged in the reverse trend of ε. The π–π stacking between the substituted pyrrole ring of **(1)** and **(2)** led to destabilization of **TS-II**, whereas the H…B between the substituted pyrrole ring and water caused to stabilization of **TS-I**. These results exhibited more sensitive of the stereoselective complex to stabilizing effects of more polar solvent *via* (D.-D.I.) and (H…B) than less polar solvents or gas phase. Furthermore, this reaction was applicable to unstable fullerene **(2)**, giving an irreversible complex **(3)**, and a hetero bond (C—S) could be formed on it's surface. Thus, the resulted organofullerene **(3)** was thermodynamically stable compound because of its aromatic character. The absorption maxima (UV-vis spectra) of organofullerene **(3)** have explored using several types of solvents (gas phase, C_6H_{12}, $CHCl_3$, MeOH, and H_2O) with different polarities. The absorption maximum (λ_{max}) changed from 489.40 to 931.43 nm in gas phase, from 502.63 to 993.08 nm in cyclohexane, from 504.08 to 994.52 nm in chloroform, from 504.41 to 1000.09 nm in methanol, and from 504.80 to 1009.72 nm in water. The pyrrole group's introduction in the resulted complex brings the absorption maxima to higher values (bathochromic shift) in the more polar solvents of MeOH and H_2O.

Summary
The analysis of the harmonic vibrational frequencies at the used DFT method showed that initial structures **(1)**, **(2)** and complex **(3)** were minima on the potential energy surfaces (imaginary frequencies were absent); while for characterizing the TSs, the existence of one imaginary frequency considered initially, and then the IRC leading to the corresponding energy minima obtained. H—bonding and suitable interaction of **TS-I** in water led to stabilization of this transition state, while the π-π aromatic stacking and electrostatic interaction led to destabilization of the **TS-II**. A plausible mechanism in order to formation of product is concerted, synergistic, stereoselective and syn—cycloaddition, which is in accordance with the proposed mechanism for Diels–Alder reaction.

Acknowledgements
Authors state that no fund is used in this research.

Supporting Information Available: The IRC diagrams, UV-visible spectra, λ_{max}, NBO charge and MEP maps, structural parameters, XYZ Cartesian coordinates of the scrutinized complex (14 pages).

References

[1] E. M. Braud, M. R. Nourrisson, A. Tonnerre, C. Picot, G. LeBaut, P. Renard, B. Pfeiffer, G. Tucker, Potential inhibitors of angiogenesis. Part I: 3-(imidazole-4(5)ylmethylene)indolin-2-ones. J. Enzyme Inhib. Med. Chem. 18 (2003) 243.

[2] F. Matloubi Moghaddam, L. Hojabri, S. Taheri, P. Pirani, A Tandem Aldol-Diels-Alder Reaction Accelerated in Water: An Approach to the Catalyst-Free One-Pot Synthesis of Spiro Thio-Oxindoles. J. Iran. Chem. Soc. 7 (2010) 781.

[3] X. Cheng, J. Wei, Q. Ge, D. Xing, X. Zhou, Y. Qian, G. Jiang, The optimized drug delivery systems of treating cancer bone metastatic osteolysis with nanomaterials, Drug Delivery 28 (1) (2021) 37.

[4] (a) S. Ölgen, Comparison of some 3-(substituted-benzylidene)-1,3-dihydro-indolin derivatives as ligands of tyrosine kinase based on binding mode studies and biological assay. Arch. Pharm. Res. 29: (2006) 1006. (b) S. Ölgen, E. Akaho, D. Nebioglu, Synthesis and anti-tyrosine kinase activity of 3-(substituted-benzylidene)-1, 3-dihydro-indolin derivatives: investigation of their role against p60c-Src receptor tyrosine kinase with the application of receptor docking studies. Il Farmaco 60 (2005) 497.

[5] S.Z. Sayyed-Alangi, M. Koohi, H. Sajjadi-Ghotabadi, Computational study of solvent effects on characterizations of (E)-3-X-Indoline-2-thiones derivatives as antivirus and anticancer compounds, Bull. Korean Chem. Soc. 36 (2015) 1985.

[6] (a) F. Matloubi Moghaddam, B. Ghanbari, M. Behzadi, M. H. Baghersad, Synthesis of Tetrahydrothiopyrano[2,3–b]indole [60]Fullerene Derivatives via Hetero-Diels–Alder Reaction of C60 and α,β-Unsaturated Indole-2–thiones, J. Heterocycl. Chem. 54 (2017) 911. (b) S. Deguchi, R.G. Alargova, K. Tsujii, Stable dispersions of fullerenes, C60 and C70, in water preparation and characterization, Langmuir 17 (2001) 6013.

[7] P.G. Gassman, T.J. van Bergen, P.D. Gilbert, W.C. Jr Berkeley, General method for the synthesis of indoles, J. Am. Chem. Soc. 96 (1974) 5495.

[8] S.-Y. Tang, J. Shi, Q.-X. Guo, Accurate prediction of rate constants of Diels-Alder reactions and application to design of Diels-Alder ligation. Org. Biomol. Chem. 10 (2012) 2673.

[9] H. Prinzbach, A. Weller, P. Landenberger, F. Wahl, J. Worth, L. T. Scott, M. Gelmont, D. Olevano, B. Issendorff, Gas-Phase Production and Photoelectron Spectroscopy of the Smallest Fullerene, C20. Nature 407 (2000) 60.

[10] B. Kräutler, J. Maynollo, Diels-Alder reactions of the [60]fullerene functionalizing a carbon sphere with flexibly and with rigidly bound addends, Tetrahedron 52 (1996) 5033.

[11] (a) Z. Shariatinia, S. Shahidi, A DFT study on the physical adsorption of cyclophosphamide derivatives on the surface of fullerene C60 nanocage, J. Mol. Graph. Model. 52 (2014) 71. (b) V. Campisciano, S. Riela, R. Noto, M. Gruttadauria, F. Giacalone, Efficient microwave-mediated synthesis of fullerene acceptors for organic photovoltaics, RSC Adv. 4(108) (2014) 63200.

[12] X. Cheng, J. Wei, Q. Ge, D. Xing, X. Zhou, Y. Qian, G. Jiang, The optimized drug delivery systems of treating cancer bone metastatic osteolysis with nanomaterials, 28 (2021) 37.

[13] M. Koohi, S. Soleimani-Amiri, M. Shariati, Novel X- and Y-substituted heterofullerenes X4Y4C12 developed from the nanocage C20, where X = B, Al, Ga, Si and Y = N, P, As, Ge: a comparative investigation on their structural, stability, and electronic properties at DFT, Struct. Chem. 29(3) (2018) 909.

[14] H. Ueno, H. Kawakami, K. Nakagawa, H. Okada, N. Ikuma, S. Aoyagi, K. Kokubo, Y. Matsuo, T. Oshima, Kinetic Study of the Diels−Alder Reaction of Li+@C60 with Cyclohexadiene: Greatly Increased Reaction Rate by Encapsulated Li+, J. Am. Chem. Soc. 136 (2014) 11162.

[15] (a) M. Asnaashariisfahani, E. Abdulkareem Mahmood, M. R. Poor Heravi, S. Habibzadeh, A. G. Ebadi, S. Mohammadi-Aghdam, Solvent effect on cycloaddition of C20 nanofullerene with indoline-2-one, at DFT, J. Phys. Org. Chem. 35 (2022) e4354. (b) A. A. B. Yosef Kinani, E. Abdulkareem Mahmood, S. M. Shoaei, M. R. Poor Heravi, S. Habibzadeh, A. G. Ebadi, I. Amini, E. Vessally, The chemical reaction of thioindole and [20] fullerene and the use of DFT to estimate some quantum chemical descriptors, J. Sulfur Chem. 44 (1) (2023) 52. (c) J.

Azamat, M. R. Poor Heravi, S. Habibzadeh, A. G. Ebadi, S. M. Shoaei, E. Vessally, Hetero Diels–Alder cycloadduct of Anti-Tumor (E)-3-X-indoline-2-thiones with C20 fullerene as drug delivery in solution vs. gas phase: A DFT survey, Inorg. Chem. Commun. 139 (2022) 109353.

[16] (a) M. W. Schmidt, K. K. Baldridge, J. A. Boatz, S. T. Elbert, M. S. Gordon, J. H. Jensen, S. Koseki, N. Matsunaga, K. A. Nguyen, S. J. Su, T. L. Windus, M. Dupuis, J. A. Montgomery, General atomic and molecular electronic structure system, J. Comput. Chem., 14 (11) (1993) 1347. (b) A. L. Sobolewski, W. Domcke, Ab Initio Investigation of the Structure and Spectroscopy of Hydronium−Water Clusters, J. Phys. Chem. A 106 (2002) 4158.

[17] (a) A. D. Becke, Density-functional exchange-energy approximation with correct asymptotic behavior, Phys. Rev. A 38 (1988) 3098. (b) A. D. J. Becke, Density-functional thermochemistry. III. The role of exact exchange, Chem. Phys. 98 (1993) 5648. (c) C. Lee, W. Yang, R. G. Parr, Development of the Colle-Salvetti correlation-energy formula into a functional of the electron density, Phys. Rev. B 37 (1988) 785. (d) A. D. Becke, Density-functional thermochemistry. IV. A new dynamical correlation functional and implications for exact-exchange mixing, J. Chem. Phys. 104 (1996) 1040.

[18] M. J. Frisch, J. A. Pople, J. S. Binkley, Self-Consistent Molecular Orbital Methods 25: Supplementary Functions for Gaussian Basis Sets, J. Chem. Phys. 80 (1984) 3265.

[19] (a) C. Peng, H. B. Schlegel, Combining Synchronous Transit and Quasi-Newton Methods to Find Transition States, Israel. J. Chem. 33 (1993) 449. (b) C. Peng, P. Y. Ayala, H. B. Schlegel, M. J. Frisch, Using redundant internal coordinates to optimize equilibrium geometries and transition states, J. Comput. Chem. 17 (1996) 49.

[20] R. A. Kendall, T. H. Jr. Dunning, R. J. Harrison, Electron affinities of the first-row atoms revisited. Systematic basis sets and wave functions. J. Chem. Phys. 96 (1992) 6796.

[21] (a) F. Weinhold, E. D. Glendening, NBO 7.0 Program Manual Natural Bond Orbital Analysis Programs. J. Comput. Chem. 33 (2012) 2363. (b) F. Weinhold, Natural Bond Orbital Analysis: A Critical Overview of Relationships to Alternative Bonding Perspectives. J. Comput. Chem. 33 (2012) 2363. (c) E. D. Glendening, C. R. Landis, F. Weinhold, Natural bond orbital methods. Wiley Interdiscip. Rev. Comput. Mol. Sci. 2 (2012) 1. (d) G. Zhang, C. B. Musgrave, Comparison of DFT Methods for Molecular Orbital Eigenvalue Calculations. J. Phys. Chem. A 111 (2007) 1554. (e) F. Biegler–König, J. Schönbohm, Update of the AIM2000-Program for atoms in molecules, J. Comp. Chem. 23 (2002) 1489.

[22] S. F. Boys, F. Bernardi, The calculation of small molecular interactions by the differences of separate total energies. Some procedures with reduced errors. Mol. Phys. 19 (1970) 553.

[23] M. Ghavami, M. Koohi, A. Ahmadi, H. Zandi, M. Z. Kassaee, Diastereoselective Synthesis of N-(p-Tosylsulfonyl)-2-Phenylaziridine Over a Novel Magnetically Recyclable Cu(II) Catalyst Accompanied with the N-Inversion Assessment at DFT, Comb. Chem. High. T. Scr. 17 (2014) 756.

[24] (a) M. Koohi, S. Soleimani-Amiri, M. Shariati, Novel X- and Y-substituted heterofullerenes X4Y4C12 developed from the nanocage C20, where X = B, Al, Ga, Si and Y = N, P, As, Ge: a comparative investigation on their structural, stability, and electronic properties at DFT. Struct. Chem. 29(3) (2018) 909. (b) M. T. Baei, M. Koohi, M. Shariati, Characterization of C20 fullerene and its isolated C20-nGen derivatives (n = 1-5) by alternating germanium atom(s) in equatorial position: A DFT survey. Heteroatom Chem. 29 (2018) e21410. (c) M. T. Baei, M. Koohi, M. Shariati, Structure, stability, and electronic properties of AlP nanocages evolved from the world's smallest caged fullerene C20: A computational study at DFT. J. Mol. Struct. 1159 (2018) 118. (d) S. Soleimani Amiri, M. Koohi, B. Mirza, Characterizations of B, and N heteroatoms as substitutional doping on structure, stability, and aromaticity of novel heterofullerenesevolvedfrom the smallest fullerene cage C20: A density functional theory perspective. J. Phys. Org. Chem. 29 (2016) 514. (e) M. Koohi, S. Soleimani Amiri, B. N. Haerizade, Substituent effect on structure, stability and aromaticity of novel BnNmC20-(n+m) heterofullerenes. J. Phys. Org. Chem. 30 (2017) e3682. (f) M. Koohi, M. Z. Kassaee, M. Ghavami, B. N. Haerizade, A. A. Ahmadi, C20-nGen heterofullerenes (n = 5 - 10) on focus: a density functional perspective. Monatsh. Chem. 146 (2015) 1409. (g) M. Koohi, S. Soleimani Amiri, M. Shariati, Silicon impacts on structure, stability and aromaticity of C20-nSin heterofullerenes (n = 1 - 10): a density functional perspective. J. Mol. Struct. 1127 (2017) 522. (h) M. Koohi, M. Shariati, S. Soleimani Amiri, A comparative study on the Ge6C14 heterofullerene nanocages: a density functional survey. J. Phys. Org. Chem. 30 (2017) e3678. (i) S. Soleimani-Amiri, M. Koohi, Z. Azizi, Characterization of nonsegregated C17Si3 heterofullerenic isomers using density functional theory method. J Chin Chem Soc 65 (2018) 1453.

[25] (a) S. A. Siadati, E. Vessally, A. Hosseinian, L. Edjlali, Possibility of sensing, adsorbing, and destructing the Tabun–2D–skeletal (Tabun nerve agent) by C20 fullerene and its boron and nitrogen doped derivatives. Synthetic Met 220 (2016) 606. (b) E. Vessally, S. A. Siadati, A. Hosseinian, L. Edjlali, Selective sensing of ozone and the chemically active gaseous species of the troposphere by using the C20 fullerene and graphene segment. Talanta 162 (2017) 505. (c) E. Vessally, S. Soleimani–Amiri, A. Hosseinian, L. Edjlali, A. Bekhradnia, The Hartree–Fock exchange effect on the CO adsorption by the boron nitride nanocage. Physica E 87 (2017) 308. (d) K. Nejati, A. Hosseinian, E. Vessally, A. Bekhradnia, L. Edjlali, A comparative DFT study on the interaction of cathinone drug with BN nanotubes, nanocages, and nanosheets. Appl. Surf. Sci. 422 (2017) 763. (e) A. Hosseinian, E. Vessally, A. Bekhradnia, K. Nejati, G. Rahimpour, Benzoylethanamine drug interaction with the AlN

nanosheet, nanotube and nanocage: Density functional theory studies. Thin Solid Films 640 (2017) 93.

[26] (a) A. Hosseinian, A. Bekhradnia, E. Vessally, L. Edjlali, M. D. Esrafili, A DFT study on the central–ring doped HBC nanographenes. J. Mol. Graph. Model. 73 (2017) 101. (b) A. Hosseinian, Z. Asadi, L. Edjlali, A. Bekhradnia, E. Vessally, NO2 sensing properties of a borazine doped nanographene: A DFT study. Comput. Theor. Chem. 1106 (2017) 36. (c) K. Nejati, A. Hosseinian, A. Bekhradnia, E. Vessally, L. Edjlali, Na–ion batteries based on the inorganic BN nanocluster anodes: DFT studies. J. Mol. Graph. Model. 74 (2017) 1. (d) B. Mirza, S. Soleimani-Amiri, M. Mirza, Reaching for [6]n SiC-cyclacenes and [6]n SiC-acenes: A DFT approach. J. Phys. Org. Chem. 31 (2017) 3754. (e) E. Vessally, S. Soleimani–Amiri, A. Hosseinian, L. Edjlali, A. Bekhradnia, A comparative computational study on the BN ring doped nanographenes. Appl. Surf. Sci. 396 (2017) 740. (f) K. Nejati, A. Hosseinian, L. Edjlali, E. Vessally, The effect of structural curvature on the cell voltage of BN nanotube based Na–ion batteries. J. Mol. Liq. 229 (2017) 167. (g) L. Safari, E. Vessally, A. Bekhradnia, A. Hosseinian, L. Edjlali, A DFT study on the sensitivity of two–dimensional BN nanosheet to nerve agents cyclosarin and tabun. Thin Solid Films, 623 (2017) 157. (d) M. Koohi, H. Bastami, Structure, stability, MEP, NICS, reactivity, and NBO of Si—Ge nanocages evolved from C20 fullerene at DFT. Monatshefte für Chemie – Chem. Mont. 151 (2020) 693.

[27] (a) E. Vessally, F. Behmagham, B. Massoumi, A. Hosseinian, L. Edjlali, Carbon nanocone as an electronic sensor for HCl gas: Quantum chemical analysis. Vacuum, 134 (2016) 40. (b) S. Bashiri, E. Vessally, A. Bekhradnia, A. Hosseinian, L. Edjlali, Utility of extrinsic [60] fullerenes as work function type sensors for amphetamine drug detection: DFT studies. Vacuum, 136 (2017) 156. (c) F. Behmagham, E. Vessally, B. Massoumi, A. Hosseinian, L. Edjlali, A computational study on the SO2 adsorption by the pristine, Al, and Si doped BN nanosheets, Superlattices Microstruct. 100 (2016) 350. (d) M. Koohi, M. Ghavami, B. N. Haerizade, H. Zandi, M. Z. Kassaee, Cyclacenes and short zigzag nanotubes with alternanting Ge—C bonds: theoretical impacts of Ge on the ground state, strain, and band gap. J. Phys. Org. Chem. 27 (2014) 735.